Title: Cytoskeletal Tension Regulates Mesodermal Spatial Organization and Subsequent Vascular Fate
Short Title: Tension and Density Regulate Stem Cell Organization

*Quinton Smith[1], *Nash Rochman[1], Ana Maria Carmo[1], Dhruv Vig[1], Xin Yi Chan[1], Sean Sun[2]^, Sharon Gerecht[1,3]^

[1]Department of Chemical and Biomolecular Engineering, Physical Sciences-Oncology Center and the Institute for NanoBioTechnology, Johns Hopkins University, Baltimore, MD 21218. [2]Department of Mechanical Engineering, Physical Sciences-Oncology Center and the Institute for NanoBioTechnology, Johns Hopkins University, Baltimore, MD 21218. [3] Department of Materials Science and Engineering, Johns Hopkins University, Baltimore, MD 21218

*Authors Contributed Equally to this Publication
^co-corresponding to: ssun@jhu.edu; gerecht@jhu.edu

www.pnas.org/cgi/doi/10.1073/pnas.1808021115

SI Materials and Methods

hiPSC Expansion

Experiments were conducted using the BC1 hiPSC cell line (1, 2). Undifferentiated hiPSCs were expanded on an inactivated layer of mouse embryonic fibroblasts (MEF) in media containing 80% ES-DMEM/F12, 20% knockout serum and 10 ng/mL of bFGF. in a humidified incubator set to 37 °C and 5 % CO_2. Stem cells were routinely tested for mycoplasma contamination in 3-month intervals, karyotyped once a year, and stained for markers to ensure pluripotency.

hiPSC Differentiation

Activated micropatterned glass coverslips (CYTOO) were coated with collagen IV (Corning) at 50 µg/mL for 1 hour at room temperature. Following coating, samples were washed with 1X PBS and allowed to air dry for at least 20 minutes. hiPSCs cultured on MEF were collected using EDTA, strained with a 40 µm strainer mesh, re-suspended and seeded in media containing α-MEM/DMEM, 10% FBS and 0.1 % β-Mercaptoethanol (Diff Media), supplemented with 10 µM Y-27632 (StemCell Technologies), at $1x10^6$ per micropatterned coverslip. After 4 hours of attachment, Y-27632 was removed or retained as outlined in the text, and fresh Diff Media was replaced. After 48 hours of culture, cells were fixed for immunofluorescence staining.

To induce early vascular cell (EVC; specification containing a bi-potent population of endothelial cells (CD31+/VECad+) and pericytes (PDGFR-β+/SM22α +), seeded micropatterns were cultured in Diff Media, for a total of six days with media changed every other day. On day six of differentiation, media was switched to EC Diff Media, containing complete Endothelial Growth Media (EGM), supplemented with 10 µM TGFβ-inhibitor and 50 ng/mL of VEGF as previously described (3-7). Media was changed every other day until day 12 of differentiation, in which they were fixed and stained to access the degree of EVC specification.

Immunofluorescent Staining

Cells cultured on micropatterned surfaces were washed with 1 X PBS, then fixed for 20 minutes with 3.7% paraformaldehyde (PFA). PFA was removed, and the samples were then washed three times with 1 X PBS. Following washing the surfaces, cells were permeabilized with 0.1% Triton X-100 for 10 minutes. Samples were washed then incubated with 1 % BSA solution for one hour at room temperature. Subsequently, micropattern surfaces were incubated with primary antibodies overnight at 4°C, then secondary conjugated for 1 hour (SI Appendix, Table S1). DAPI was incubated for 3-5 minutes to mark nuclei. Finally, the stained micropatterns were inverted and mounted on glass coverslips using Mounting Media (Thermo Fisher Scientific).

Imaging

Images were acquired using a Zeiss 780 confocal microscope fit with a 10x objective. To image the entire micropattern arena, title image acquisition was used in addition to a Z-stack (5 µm interval slices) in three channels corresponding to DAPI, Alexa Fluor 546, and Alexa Fluor 488.

Image Quantification

We report Brachyury expression as the nuclear / cytoplasmic intensity ratio: a measure which is independent of the imaging conditions and easily compared across multiple biological replicates, and the arbitrary threshold of 0.5 standard deviations above the mean was selected to indicate the positive ensemble. To quantify the degree of cytoskeletal tension imposed by

micropattern geometry, integrated pixel intensities of RhoA or pMLC were normalized per geometric area. Each marker was quantified in at least two independent micropattern experiments.

Support Vector Machine Learning

For a walkthrough of the protocol, please see Supplementary Methods. The immunofluorescence images were smoothed to obtain local population averages. First two masks were obtained: one for the patterns, or the entire field for the unconfined case, and a second for the nuclei. Both the pattern and nuclear masks were obtained by identifying bright regions of the field when compared to background intensity. Given the appropriate masks, each channel was averaged within discs of a few cell diameters in radius. For day 2 images, the three channels of interest for each experiment were mean RhoA or mean pMLC normalized by cell density, cell density, and Brachyury Expression. Mean RhoA and PMLC expression are local population averages within the disk. The local cell density was reported as the fraction of each disk occupied by portions of the nuclear mask. Brachyury Expression was similarly calculated by taking the local spatial average of intensities. For day 12, the channels of interest were again cell density with the addition of distance to the perimeter of the pattern, SM22α, and VECad which were similarly reported as spatial averages. Note unlike RhoA and pMLC which are normalized by cell density, SM22α, and VECad are not normalized by cell density. For day 2, two class learning was accomplished between low and high (0.5 standard deviations above the mean) Brachyury regions. For day 12, multiple SVM's were trained to 100 masks for both the SM22α, and VECad channels, predicting each percentile of the expression landscape. Performance statistics (sensitivity and specificity) were calculated. For day 2, the predictive power of only cell density, only pMLC/RhoA expression, and dual channels were contrasted. Note a radial box function (Gaussian) kernel was used within the implementation of the SVM. The MATLAB functions "fitcsvm" and "predict" were utilized.

SI Figures

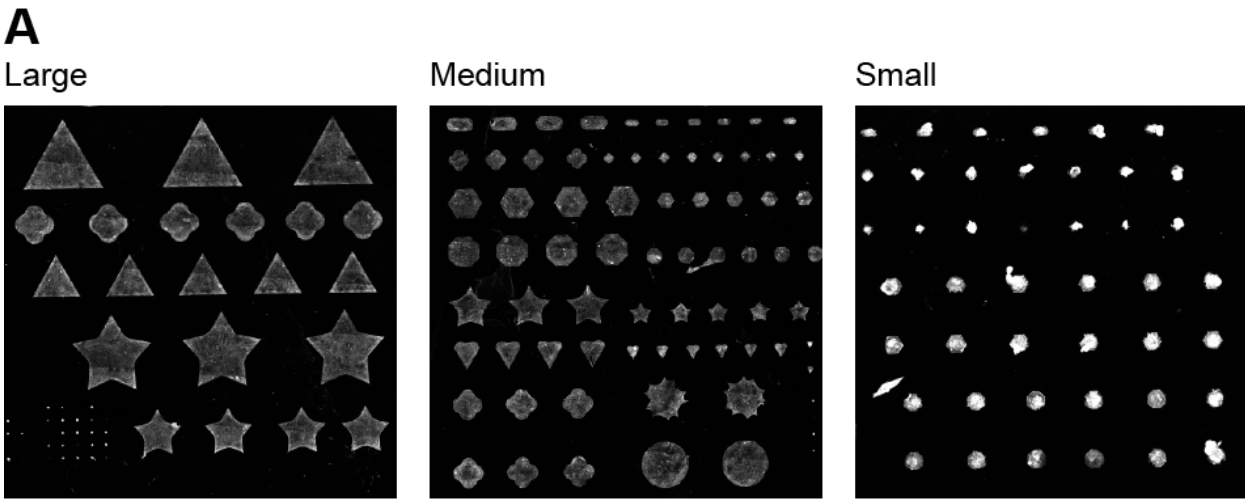

B

Shapes	Dimensions (μm)
Circle	10/30/40/50/100/300/600/1000 diameter
Isosceles Triangle	62.5/125/250/501 equal lengths
Equilateral Triangle	67/134/269/538/807/1346 lengths
Square	88/117/354 length
Square + 2 semi-circles	43/87/174 height
Square + 4 semi-circles	33/66/132/197/328 square length
Hexagon	54/109/219
Octagon	42/82/164
Heart (1 equilateral triangle + 2 semi-circles)	80/160/321
Star (5 equilateral triangles + 1 pentagon)	22.5/45/90/180/270/449
Star (10 pointed)	16.7/67/133.9 pointed edge

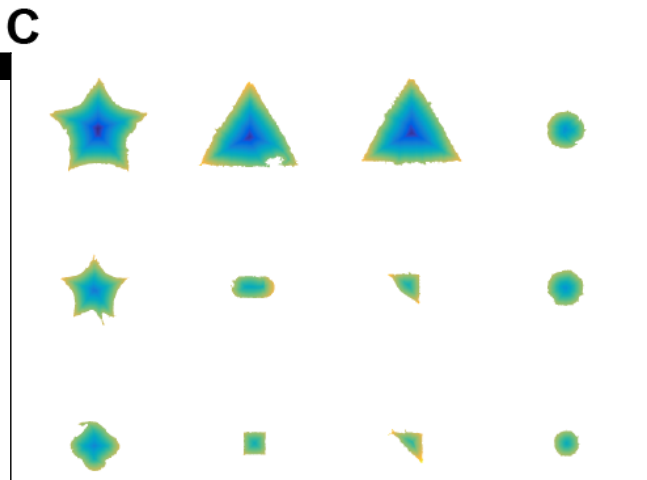

Figure S1: Micropattern Design. (A) Representative images of large (1.0 x10^5 - 2.5 x10^5 μm^2), medium (1.0 x10^4 - 6.0 x10^4 μm^2) and small micropatterns (4.0 x10^3 - 1.0 x10^4 μm^2) used in this study are displayed. Micropatterns (manufactured by CYTOO^{TM}) were designed to impose varying levels of cytoskeletal tension by creating multiple geometries (e.g. squares, triangles, stars, hexagons etc.) of different sizes. To prevent any morphogen cross-talk between the micropatterns, a gap distance of 200 μm was introduced between each shape. (B) Table outlining the shapes and corresponding dimensions of the micropatterned geometries. (C) Pseudo-curvature for a variety of patterns. Cells attached at the boundary of a pattern express higher levels of pMLC/RhoA than those near the center of a pattern due to higher cytoskeletal tension. One explanation for the increased tension is the larger difference in osmolarity between the media and the interior of the cell than the interiors of two neighboring cells. In particular, points on the edge of patterns that are near cusps highlight this effect as cells in these regions have few neighboring cells. To illustrate this phenomenon, we constructed the following function we call pseudo curvature. First the distance to the shape's perimeter PD is calculated. Next, a neighbor distance function for each point on the perimeter defined to be:

$$ND = \frac{1}{L * ED}\sum_{j=1}^{L}\sqrt{\left(\boldsymbol{x} - x_j\right)^2 + \left(\boldsymbol{y} - y_j\right)^2}$$

where $[\boldsymbol{x}, \boldsymbol{y}]$ are the points which make up the shape's perimeter; L is the number of points in the shape's perimeter; and ED is the equivalent diameter of the shape (the diameter of a circle with the same area as the shape) is calculated. This function is large for points far away from the majority of the pattern e.g. points on a star. The neighbor distance and distance to the shape's perimeter are then normalized by the maximum and minimum values obtained for all shapes in the ensemble:

$ND \rightarrow \left(ND - \min_{All\ Shapes}(ND)\right)/\left(\max_{All\ Shapes}(ND) - \min_{All\ Shapes}(ND)\right)$ and

$PD \rightarrow \left(PD - \min_{All\ Shapes}(PD)\right)/\left(\max_{All\ Shapes}(PD) - \min_{All\ Shapes}(PD)\right)$.

The pseudo curvature is then defined for every point within each shape to be: $PC = (r + ND)(1 - PD)$ where $r = 1.5$.

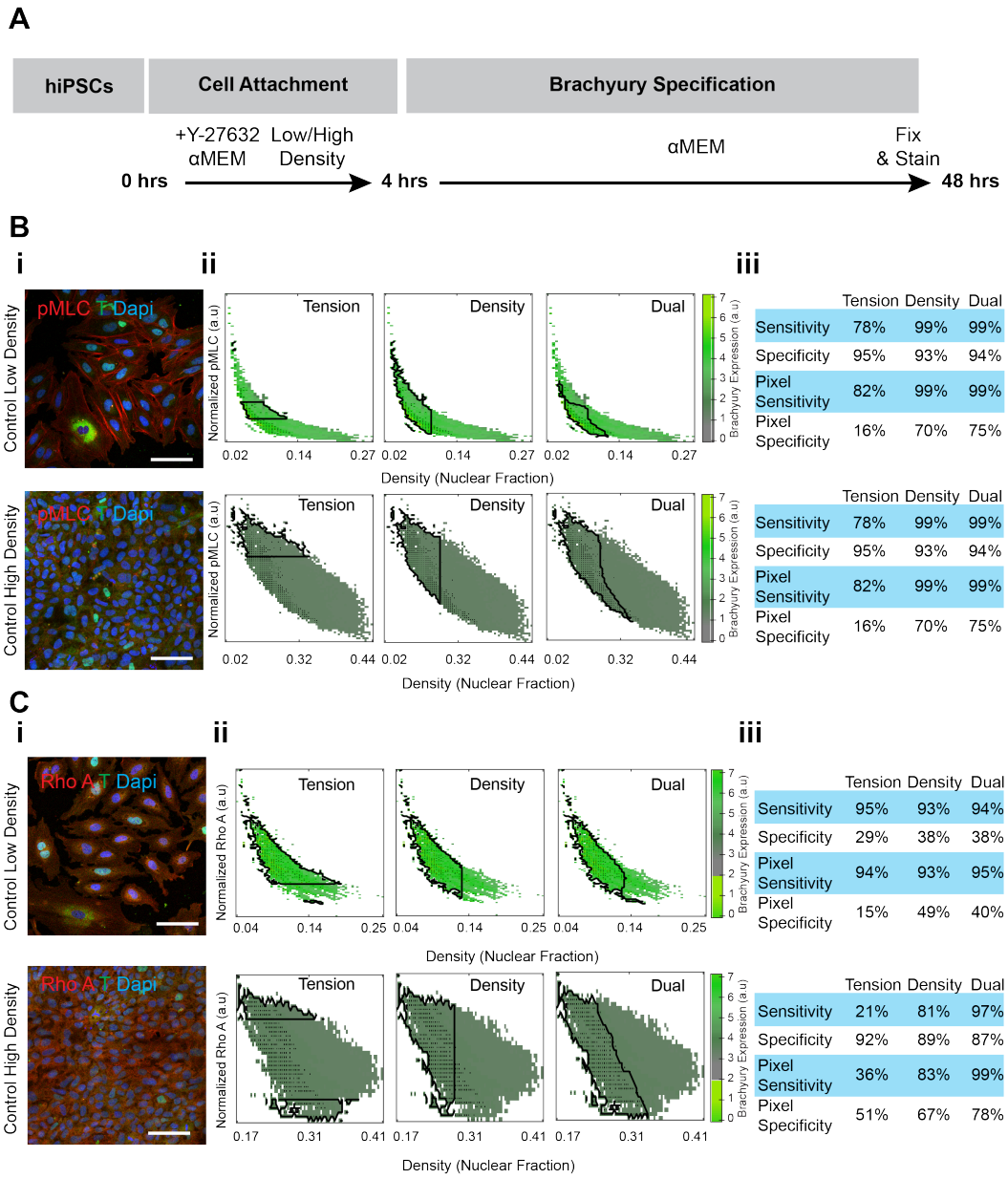

Figure S2: SVM for pMLC/RhoA Expression and Density for Brachyury Expression in Unconfined Differentiation (A) Schematic describing mesoderm induction in unconfined domains. Control samples for (Bi) pMLC and (Ci) RhoA expression at low and high-density fields separately analyzed (pMLC shown combined in the main text in Fig 1). (Bii, Cii) Brachyury expression is qualitatively much higher in low density cases (corresponding to higher levels of pMLC/RhoA as shown in the main text. Interestingly, the phase space is narrower in the low-density cases suggesting cell density and tension have a stronger co-dependence. (Biii, Ciii) While Brachyury expression gradient shows a similar trend across the phase space, cell density remains as the strongest SVM Brachyury predictor. Scale bars, 100 μm.

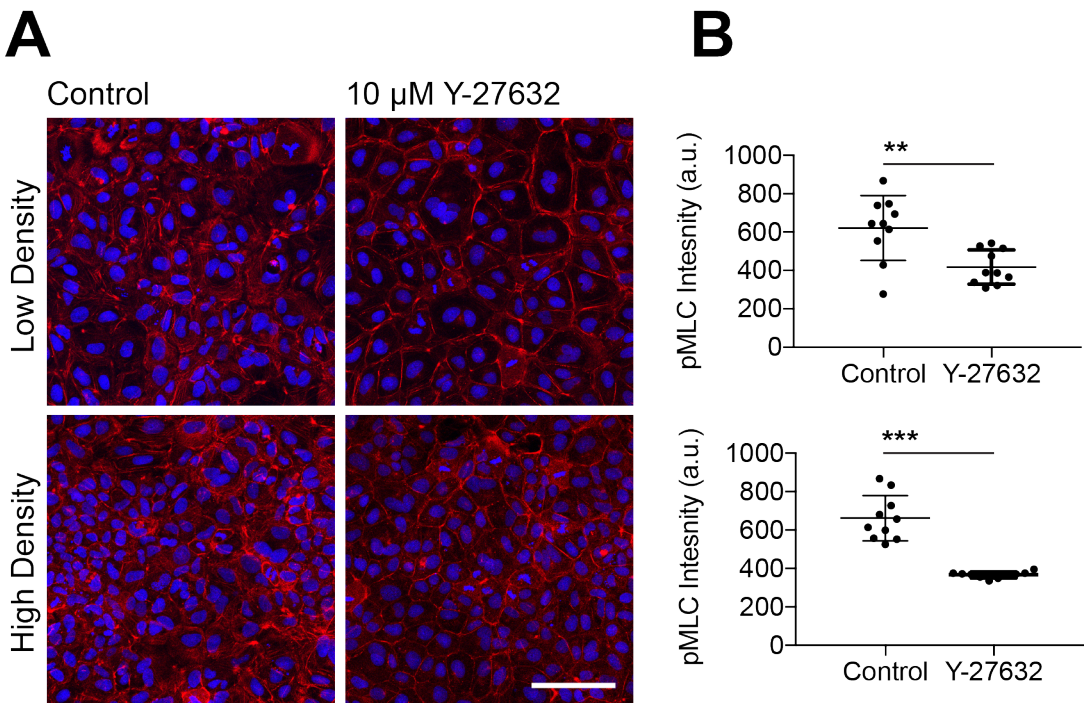

Figure S3. RhoA/ROCK Inhibition with Y-27632 Decreased pMLC Expression. (A) Representative images of hiPSCs seeded at low and high densities after 48 hours stained for pMLC, with and without 10 μM Y-27632. (B) Quantification of mean pMLC expression shows decreased intensity with RhoA/ROCK inhibition. Data quantified from 10 fields of view. Statistics acquired via an un-paired t -test where **$p < 0.05$, ***$p < 0.001$.
Scale bar is 100 μm.

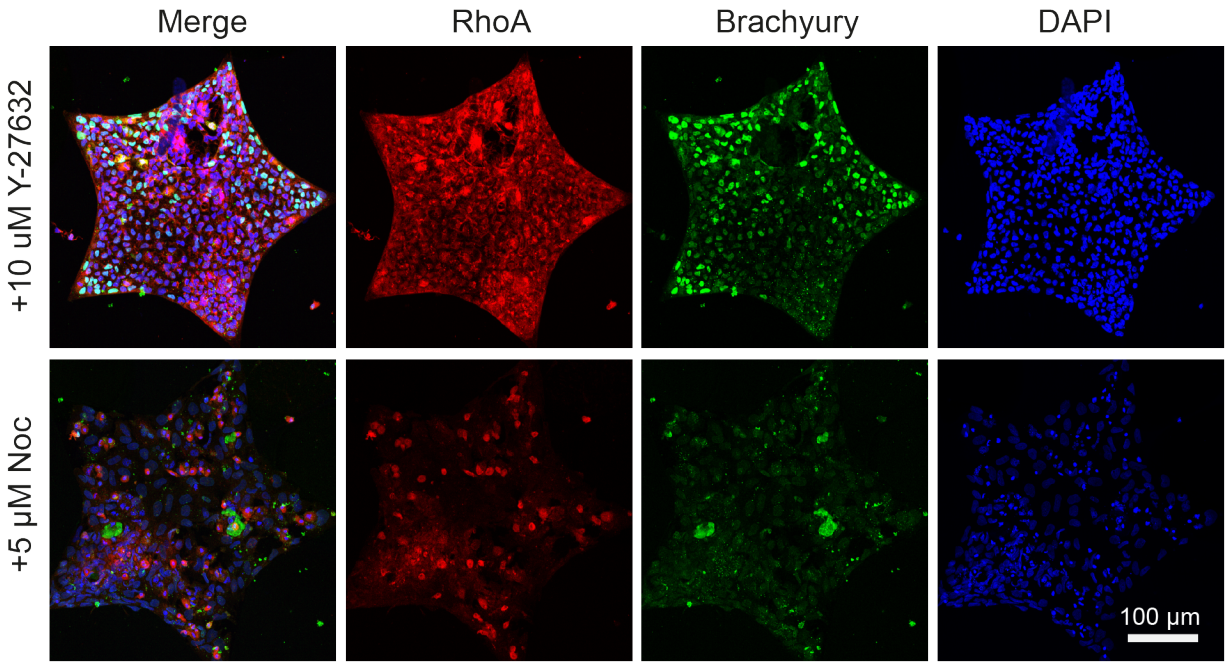

Figure S4: Cytoskeletal Inhibition of Micropatterned Domains. Fixed micropatterns after 48 hours of differentiation as a function of RhoA/ROCK inhibition with Y-27632 (top) and microtubules with Nocodazole (bottom). While disruption of microtubules also results in the disruption of mesodermal patterning on the edge of the micropatterns, local nuclear deformations were not permissive to our image segmentation algorithms.

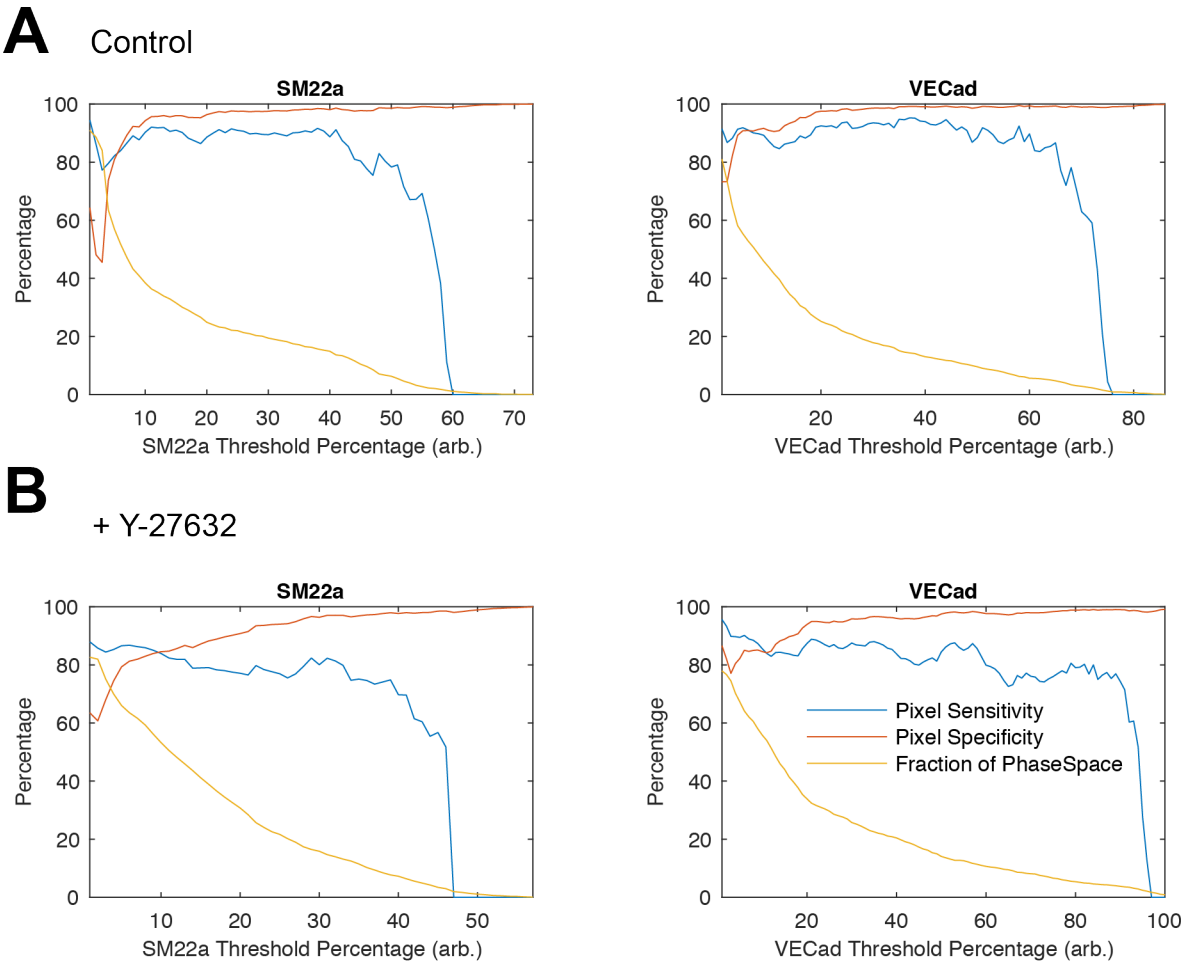

Figure S5: Specificity and Sensitivity Analysis on Day 12. The unweighted pixel sensitivity/specificity are shown for regions bounded below by each percentile of the VECad and SM22α phase spaces (X Threshold Percentage) for (A) control and (B) with Y-27632. Additionally, the fraction of the phase space is displayed. As the percentile increases, the fraction of the phase space decreases and subsequently sensitivity decreases while specificity increases.

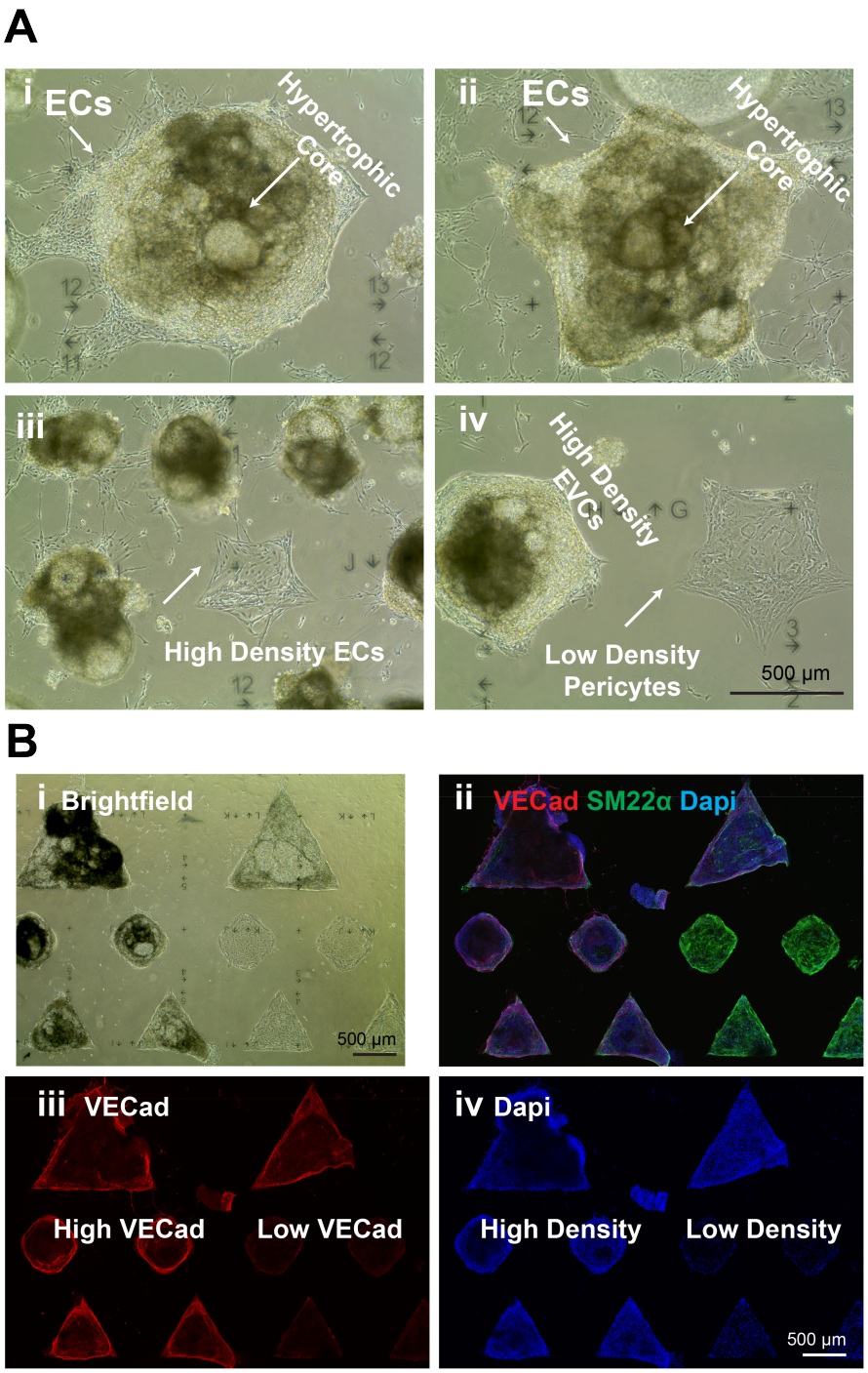

Figure S6: Control Day 12 Micropattern Vascular Specification. (A i, ii) Bright-field images. We can see in the highest density cases, a ring of ECs (identified by white arrows) around a hypertrophic core of differentiated cells. (A iii) In cases where there is high density in smaller micropatterns, we can observe the entire patterns are occupied by ECs, (Aiv) while in small micropatterns with low density morphologically we can see pericytes. (B) Representative differences in early vascular specification showing (Bi) bright-field and immunofluorescence images (B,ii-iv).

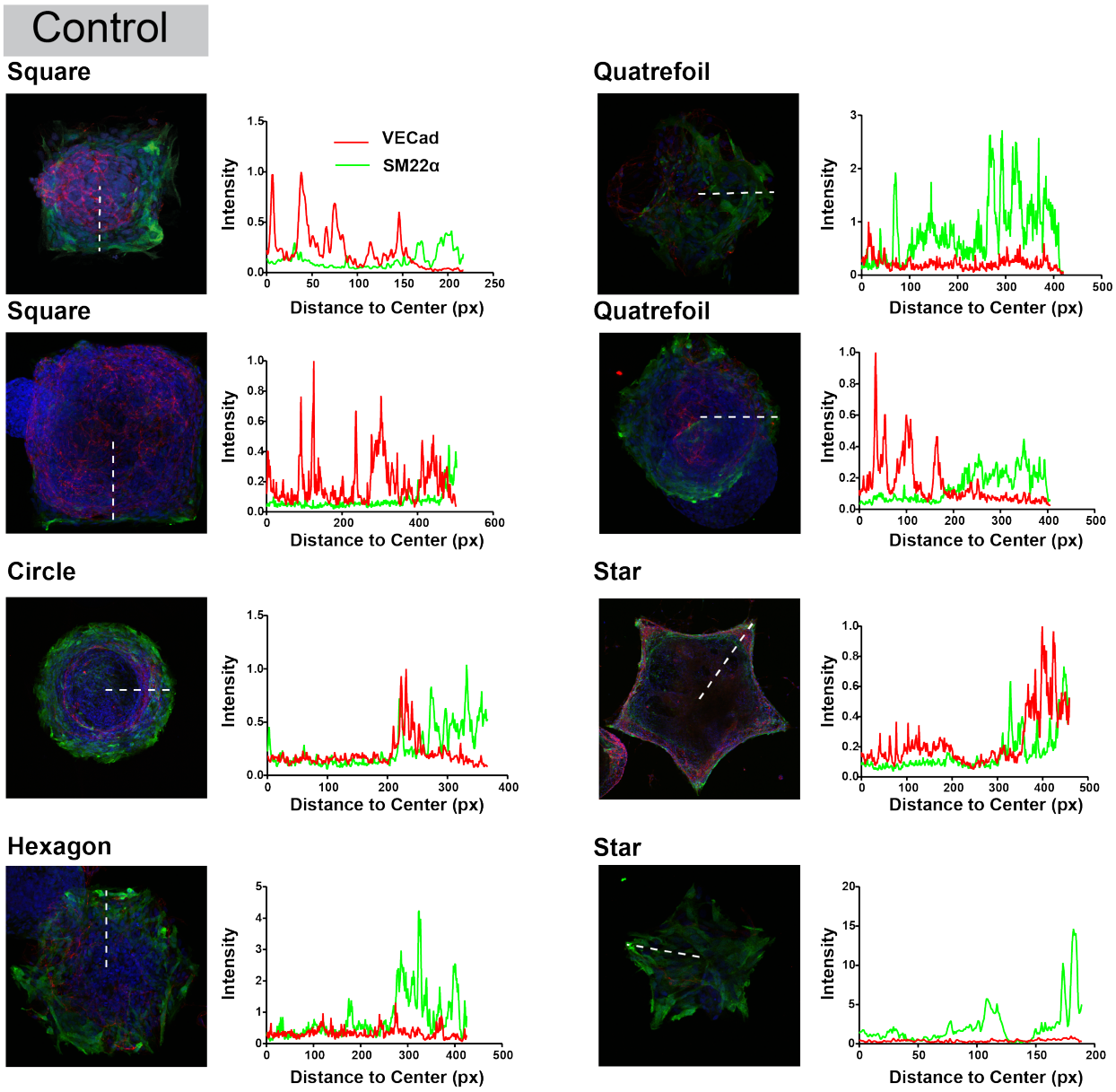

Figure S7: Example fluorescent traces of SM22α (green) and VECad (red) expression in control micropatterns at day 12 of differentiation.

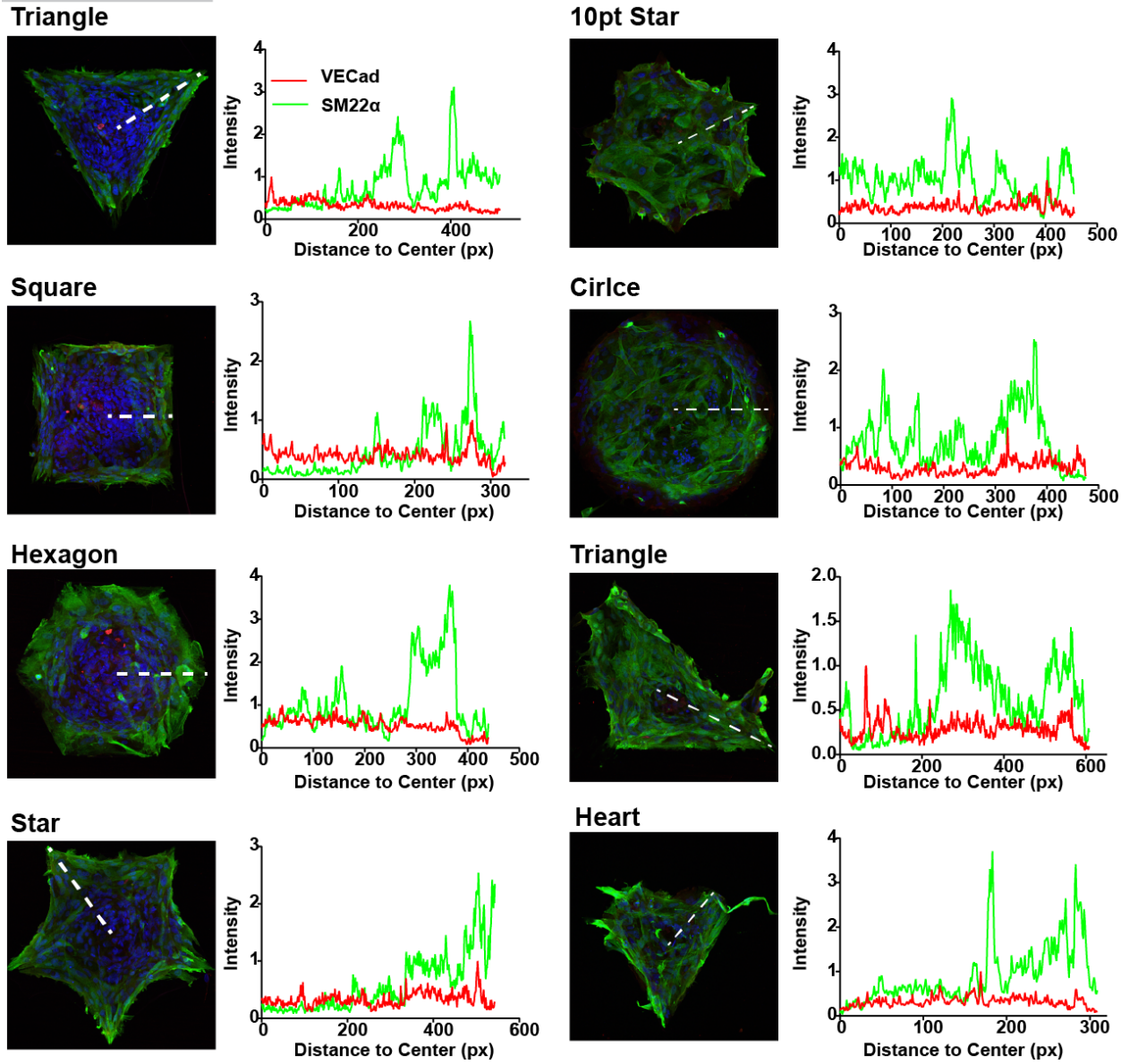

Figure S8: Example fluorescent traces of SM22α (green) and VECad (red) expression in Y-27632 micropatterns at day 12 of differentiation.

Supplementary Methods

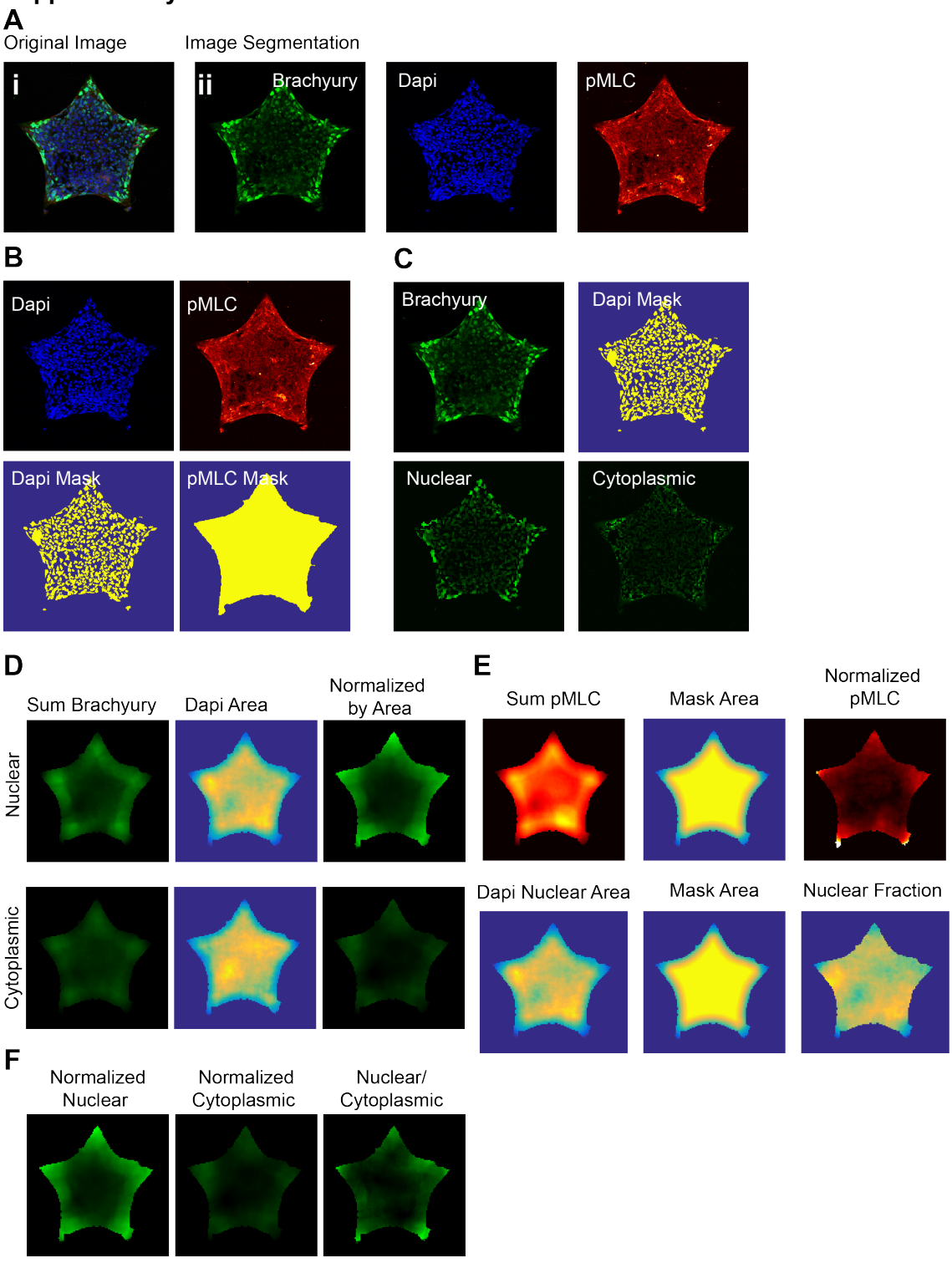

Figure S9: Image Processing for Day 2 Micropatterns. (Ai) First the original image is displayed and the image is segmented where the Dapi are blue, Brachyury in green and pMLC/RhoA in red. (B) The Dapi and pMLC/RhoA channels are then used to construct the

nuclear and pattern masks respectively. Note in the unconfined case, the pattern mask is replaced by a cell mask in the low-density case or the entire field of view in the high-density case. The Dapi mask is then used to calculate the approximate number of cells within each pattern based on the total area occupied by nuclei and the approximate nuclear area. Next, four channels – Dapi mask, pattern mask, Brachyury, and pMLC/RhoA – are resized by a factor of five. This step is done to speed up the computation roughly 25-fold and does not impact the results since we are not concerned with small subcellular detail – only distinguishing between nucleus and cytoplasm. (C) After this step, the Brachyury channel is separated into its nuclear and cytoplasmic components based on the masks. (D) Next, the local sum over an area of a few cells is calculated for six channels – nuclear area, cytoplasmic area, mask area, nuclear Brachyury, cytoplasmic Brachyury, and (E) pMLC/RhoA. Following this step, normalized channels are constructed: sum nuclear area is divided by sum mask area; sum nuclear Brachyury is divided by sum nuclear area; sum cytoplasmic Brachyury is divided by sum cytoplasmic area; and sum pMLC/RhoA is divided by sum mask area. This yields the nuclear fraction channel and normalized pMLC/RhoA expression channel used for the subsequent SVM analysis in addition to the nuclear Brachyury intensity and cytoplasmic Brachyury intensity. (F) Finally, our measure of the Brachyury expression is calculated by taking the ratio of the nuclear and cytoplasmic intensities.

Support Vector Machine Workflow

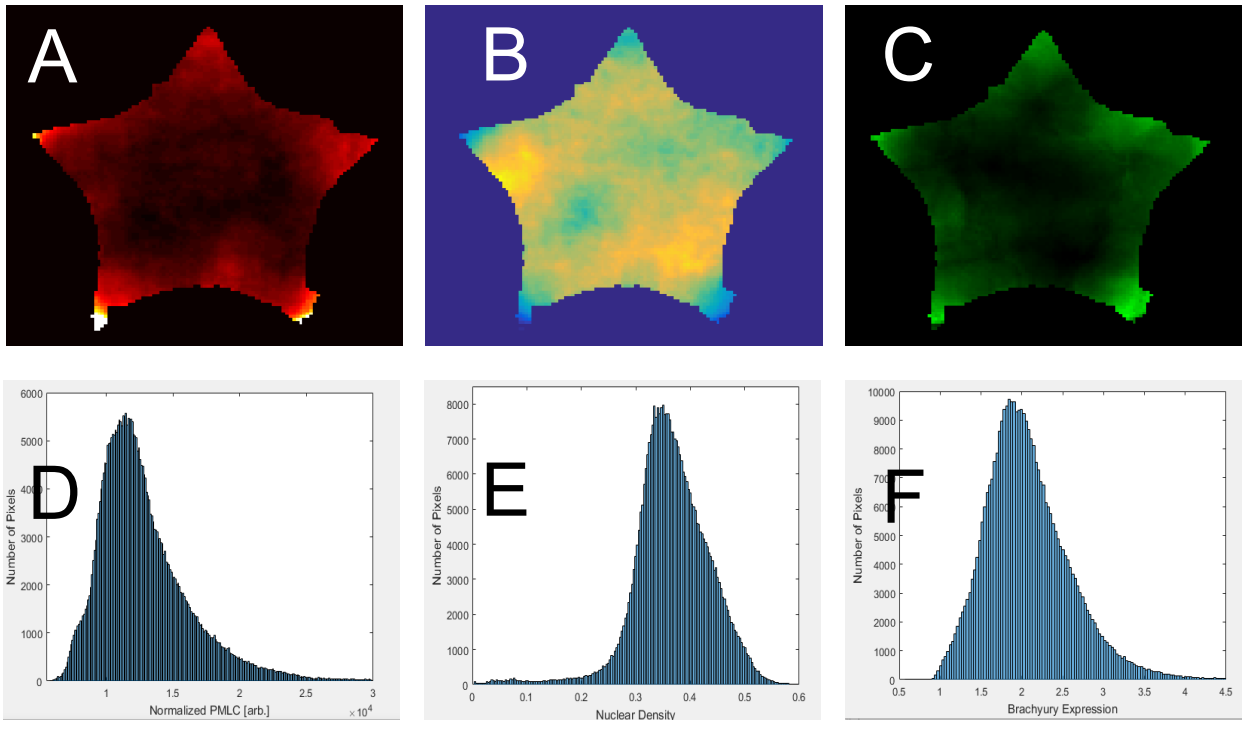

Figure S10. Aggregation of Channels Used for SVM: First, the three channels used for SVM - normalized pMLC/RhoA expression (A), nuclear density (B), and Brachyury expression (C) – are aggregated across many patterns. Patterns are excluded based on density and size: small patterns, and overgrown patterns (where cells are clustered in 3D) are removed due to their poor segmentation in the Dapi channel. (Note that when multiple biological replicates were combined for the figure in the main text, the pMLC channel was scaled by the mean intensity on each day to account for variability in staining and imaging parameters.)

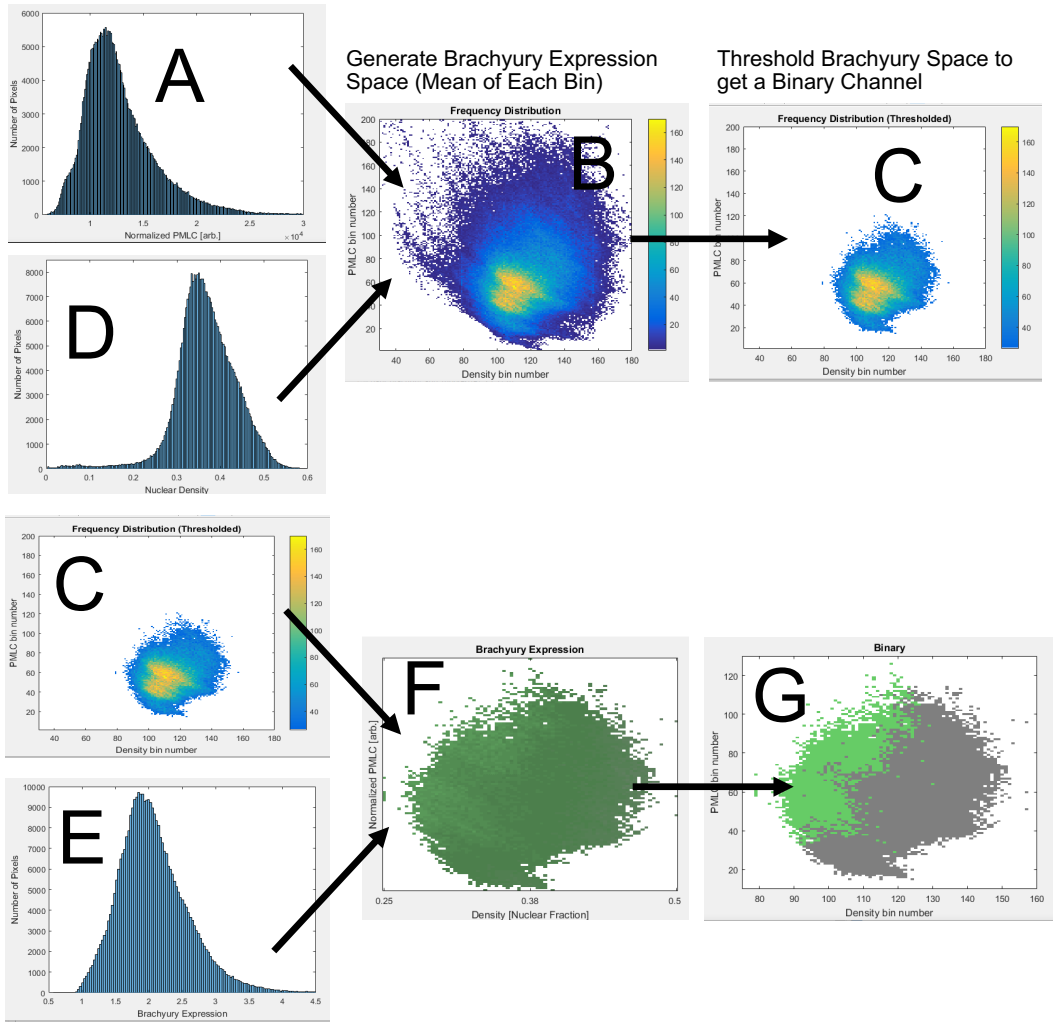

Figure S11. Generation of the Brachyury (T) space: The aggregated channels are binned and a frequency distribution (B) is constructed in pMLC/RhoA (A) and nuclear density space (D). That space is then limited to only high frequency regions (C). For each point in the reduced phase space, the corresponding Brachyury Expression values (E) are averaged to generate the Brachyury expression space (F). That space is thresholded to obtain a binary indicating the high and low Brachyury expressing regions (G).

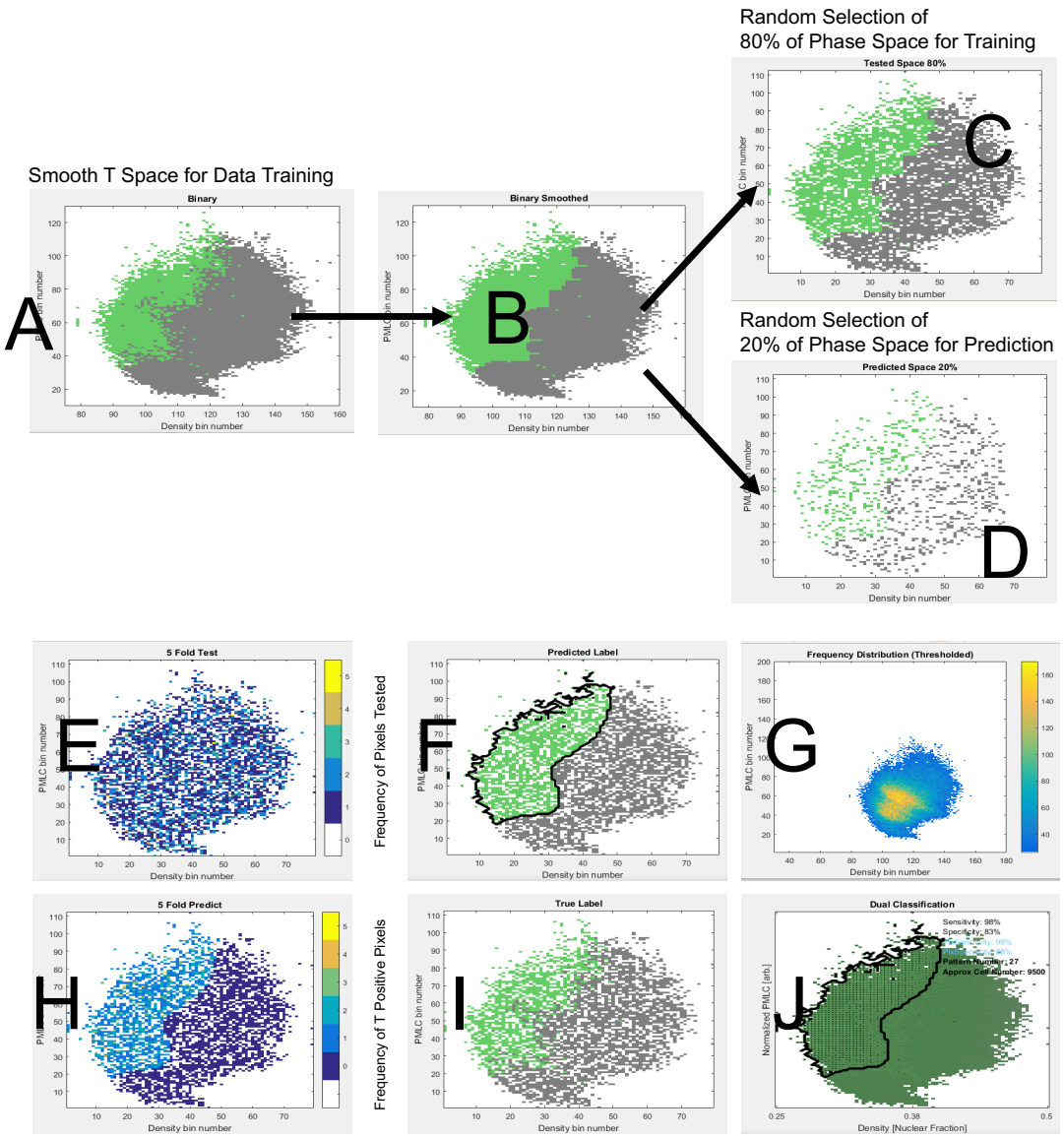

Figure S12. SVM Analysis: The high Brachyury space (A) is then smoothed to generate the training data used for SVM analysis (B). Three channels - normalized PMLC/RhoA expression, nuclear density, and binary Brachyury expression – are then used by implementing the MATLAB fitcsvm function where “Standardize” is set to true, and data is weighted based on the frequency distribution. Additionally, “BoxConstraint”, which impacts the cost associated with misclassifying training data, is set to 1. The “rbf”, radial basis function (Gaussian), kernel is selected and 80% of the data (C) is used to predict the remaining 20% (D) using the MATLAB function “predict”. This process is repeated five times and the points are randomly selected allowing for multiple classifications of the same point in the phase space, while some others remain untested (E,F). A binary is generated for the tested space (any point identified as high Brachyury in at least one run is considered positive)F. The accuracy measures (weighted sensitivity, weighted specificity, unweighted pixel sensitivity, and unweighted pixel specificity) are calculated comparing the tested binary (F) and the true binary (I) from the training data where weights are drawn from the frequency space (G). Finally, the predicted boundary is constructed, filling holes, smoothing edges, and displayed over the Brachyury expression space where true points are identified with dots (J).

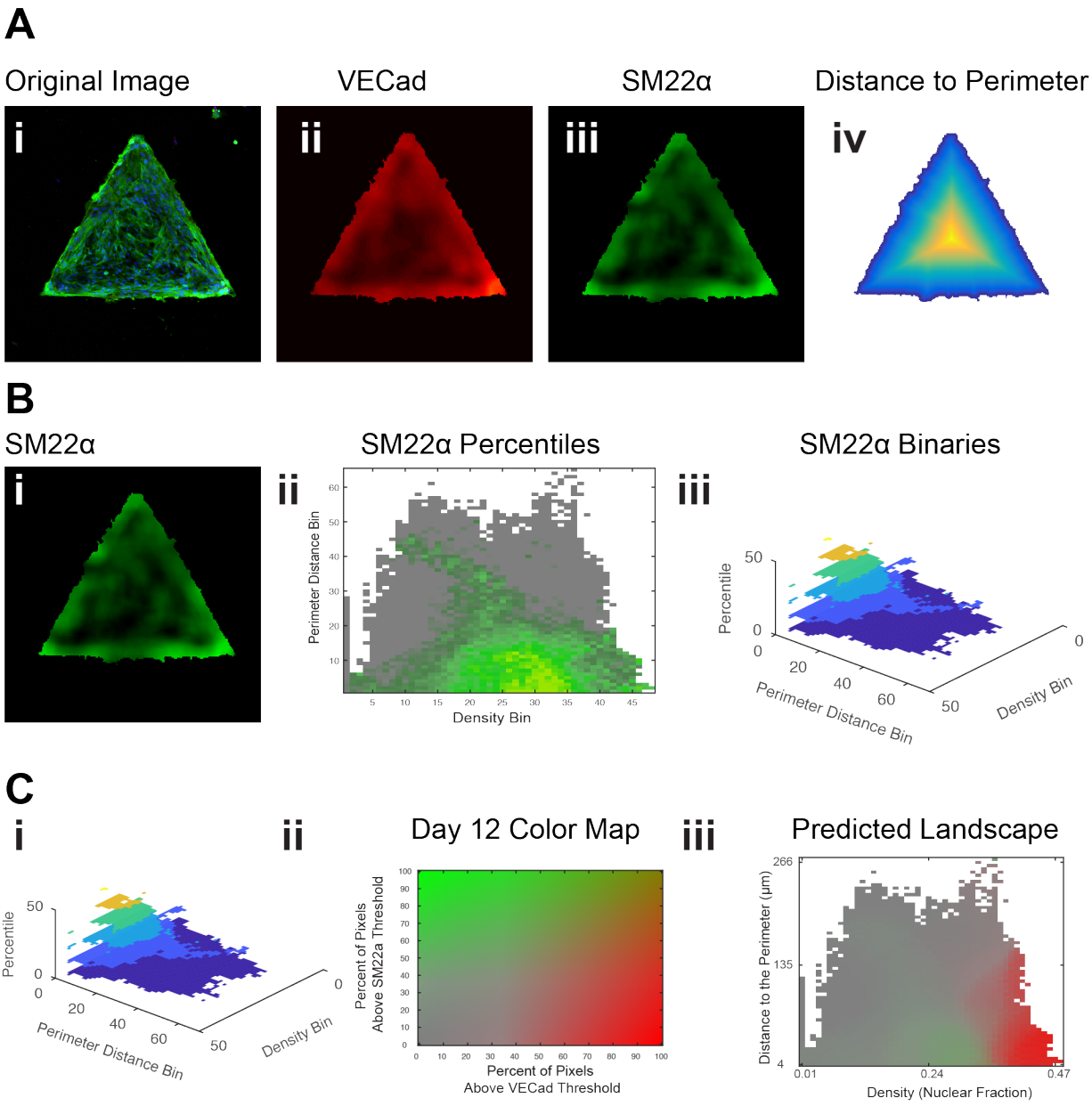

Figure S13. Day 12 Support Vector Machine Learning to Predict Vascular Fate: This process is similar to Day 2. (Ai) The original image from day 12 analysis is processed. In this case, Brachyury expression is replaced by total VECad (Aii) and SM22α (Aiii) expression which are not normalized by cell number. PMLC/RhoA is similarly replaced with distance from the perimeter of the pattern (Aiv). After perimeter distance, and nuclear density are aggregated in the same fashion as is done for PMLC/RhoA and nuclear density for Day 2, the VECad and SM22α space is generated (SM22α example shown in Bii). Here rather than taking the average of all the pixels that contribute to each point within the space, the percent of contributing pixels which are above the threshold value for each channel is calculated. Binary masks (SM22α example shown Biii) are then generated for every percentile (0-99) of both spaces and multiple

SVMs are trained. Here, a simple 2-fold cross validation is accomplished taking half the points as training data and testing the other half for a total of 400 SVMs constructed. Now each point in the phase space is identified with two numbers, VECad percentile and SM22α percentile. The 2D Day12 colormap (Ciii) is then used to visualize both the predicted (Ciii) and measured landscape of VECad and SM22α expression.

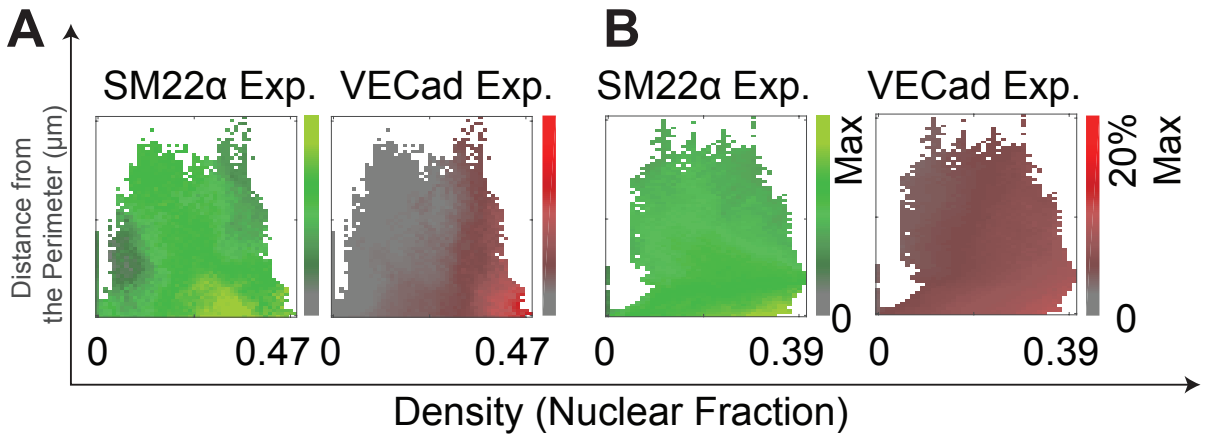

Figure S14: (A) Control micropatterns show clear measurable and distinct expression patters of SM22α and VECad expression as a function of density and distance from the perimeter. (B) The gradient of SM22α and VECad is much more uniform throughout the phase space under Y-27632.

Supplementary Tables

Experiment		Dual Sensitivity	Dual Specificity	Dense Sensitivity	Dense Specificity	pMLC Sensitivity	pMLC Specificity
n =1 (68 patterns)	Normalized	97	99	93	98	42	97
	Pixels	99	90	98	83	74	27
n =2 (93 patterns)	Normalized	98	98	49	98	76	98
	Pixels	98	87	69	72	81	45
n =3 (27 patterns)	Normalized	97	85	81	82	43	76
	Pixels	98	88	74	69	57	53
Combined pMLC	Normalized	96	99	92	99	50	99
	Pixels	98	92	97	81	81	26
Mean	Normalized	97.3	94	74.3	92.7	53.7	90.3
	Pixels	98.3	88.3	80.3	74.7	70.7	41.7
Standard Deviation	Normalized	0.58	7.81	22.75	9.24	19.3	12.42
	Pixels	0.58	1.53	15.5	7.37	12.34	13.32

Table S1: Sensitivity and Specificity for Individual Biological Repeats from Day2. Here the sensitivities and specificities for each biological repeat are shown separately along with the combined results of all three repeats pooled and the mean/standard deviation of the separate biological repeats. The Normalized values correspond to the weighted results (labelled simply "Specificity/Sensitivity" in the main text). Pixel values correspond to statistics unweighted by the frequency of each pixel observed.

Antibody	Source	Catalog #	Purpose	Host Species & Reactivity	Working Concentration
DAPI	Roche	10236276	IF	Nucleus	1:10,000
Alexa Fluor 488	Life Technologies	A-11008	IF	Goat anti-rabbit	1:1,000

Alexa Fluor 546	Life Technologies	A-10036	IF	Donkey anti-mouse	1:1,000
VECad (F-8)	Santa Cruz	Sc-9989	IF	Mouse Polyclonal	1:100
SM22α	Ab Cam	Ab 14106	IF	Rabbit anti-human	1:100
Brachyury (T)	R&D Systems	MAB20851	IF	Rabbit Monoclonal	1:200
Brachyury (T)	R&D Systems	AF2085	IF	Goat Polyclonal	1:200
Rho A	Abcam	Ab54836	IF	Mouse Monoclonal	10 µg/mL
pMLC Light Chain (Thr18/Ser19	Cell Signaling Technology	3674T	IF	Rabbit Polyclonal	1:200

Table S2: Antibodies Used in This Study. IF = Immunofluorescence

SI Movies

Movie S1: Example 1-BC1 hiPSCs were imaged for 44 hours after 4 hours attachment in the presence of 10 µM Y-27632. Cells seeded in a random fashion, are able to survey the micropattern area, grow into to the confined domains, and undergo mesodermal specification in differentiation medium.

Movie S2: Example 2 – BC1 hiPSCs differentiating on micropatterned domains.

Movie S3: Example 3 – BC1 hiPSCs differentiating on micropatterned domains.

Movie S4: Example 4 – BC1 hiPSCs differentiating on micropatterned domains.

References

1. Cheng L*, et al.* (2012) Low Incidence of DNA Sequence Variation in Human Induced Pluripotent Stem Cells Generated by Nonintegrating Plasmid Expression. *Cell Stem Cell* 10(3):337-344.
2. Chou B-K*, et al.* (2011) Efficient human iPS cell derivation by a non-integrating plasmid from blood cells with unique epigenetic and gene expression signatures. *Nature Publishing Group* 21(3):518-529.
3. Smith Q*, et al.* (2017) Compliant substratum guides endothelial commitment from human pluripotent stem cells. *Science Advances* 3(5):e1602883.
4. Kusuma S, Smith Q, Facklam A, & Gerecht S (2017) Micropattern size-dependent endothelial differentiation from a human induced pluripotent stem cell line. *Journal of Tissue Engineering and Regenerative Medicine* 11(3):855-861.
5. Chan XY*, et al.* (2015) Three-Dimensional Vascular Network Assembly From Diabetic Patient-Derived Induced Pluripotent Stem Cells. *Arteriosclerosis, Thrombosis, and Vascular Biology* 35(12):2677-2685.
6. Kusuma S, Peijnenburg E, Patel P, & Gerecht S (2014) Low Oxygen Tension Enhances Endothelial Fate of Human Pluripotent Stem Cells. *Arteriosclerosis, Thrombosis, and Vascular Biology* 34(4):913-920.
7. Kusuma S*, et al.* (2013) Self-organized vascular networks from human pluripotent stem cells in a synthetic matrix. *Proc. Natl. Acad. Sci. U.S.A.* 110(31):12601-12606.